Nanostructure of the Fibrin Clot

C. Yeromonahos,[†] B. Polack,[‡§] and F. Caton[†*]

[†]Laboratoire de Rhéologie, Centre National de la Recherche Scientifique, UMR5520, Université Joseph Fourier, Grenoble, France; [‡]Laboratoire d'Hématologie, Centre Hospitalier Universitaire, Grenoble, France; and [§]Laboratoire Techniques de l'Ingénierie Médicale et de la Complexité-THeREx, Centre National de la Recherche Scientifique, UMR5525, Université Joseph Fourier, Grenoble, France

ABSTRACT The nanostructure of the fibrin fibers in fibrin clots is investigated by using spectrometry and small angle x-ray scattering measurements. First, an autocoherent analysis of the visible light spectra transmitted through formed clots is demonstrated to provide robust measurements of both the radius and density of the fibrin fibers. This method is validated via comparison with existing small-angle and dynamic light-scattering data. The complementary use of small angle x-ray scattering spectra and light spectrometry unambiguously shows the disjointed nature of the fibrin fibers. Indeed, under quasiphysiological conditions, the fibers are approximately one-half as dense as their crystalline fiber counterparts. Further, although the fibers are locally crystalline, they appear to possess a lateral fractal structure.

INTRODUCTION

The formation of the fibrin clot is one of the major processes in blood coagulation, involving the polymerization of fibrinogen monomers into a fractal network of randomly oriented fibrin fibers. Fibrinogen is a centrosymmetric glycoprotein of high molecular mass (= 340 kDa) that has a trinodular structure $\simeq$45 nm in length and $\simeq$5 nm in diameter and a density of $\simeq$1395 g/cm^3 (e.g., (1)).

The current understanding of this polymerization process is described here. First, the enzyme thrombin cleaves the fibrinopeptides A and B from fibrinogen, which leads to the formation of half-staggered, linear protofibrils. These protofibrils subsequently aggregate into fibers of varying thicknesses that depend upon the concentration of reactants and many other external factors. Thanks to numerous studies since the 1930s, the detailed crystalline structure of the fibrinogen molecule is now well known and a large body of knowledge exists regarding its polymerization process. However, some important aspects remain largely unknown, such as the detailed nanostructure of the fibers, which is likely of particular importance for the mechanical properties of the clot. It is unclear whether the nanostructure is crystallinelike (2,3) or mainly random (4,5). The extent to which the nanostructure depends on reactants and the experimental conditions is also unknown.

The goal of this article is to provide clear answers to the above basic questions. An important step in providing these answers is to gather reliable data about the internal structure of these fibers. We will now briefly discuss the available information regarding the structure of fibrin clots and the tools most often used to study them.

Turbidimetry and light scattering

Turbidimetry (also called ''nephelometry'') is one of the first quantitative methods used to investigate the properties of blood clots. Early investigators used this method to observe the increase in the optical density of clots as they formed. Klinke (6,7) and Klinke and Elias (8) pioneered this technique in a series of articles published in the 1930s. Expanding on these findings, Ferry's work (9,10), which used turbidimetry extensively, is the keystone of the modern understanding of fibrinogen clotting. In its standard, modern implementation, turbidimetry is understood as the recording of the optical density of the clot at a single wavelength (350 nm) (11,12). The quantitative link between the opacity of the clot and its structural characteristics comes from the seminal work of Cassasa (13) followed later by that of Carr and co-workers (14–16). Carr and co-workers derived formulas that allow the extraction of structural information (radius and density) from clots scanned at many wavelengths. As we will show, while the fundamental concepts of Carr's work are valid, Carr's analysis (14,16) needs correction. More recently, several in-depth studies using small-angle light-scattering (SALS) explored the structure of fully formed or evolving clots (17–20). In particular, Ferri et al. (18,19) investigated the clot's microscale properties in catalytic conditions, i.e., when the concentration ratio of thrombin to fibrinogen is 1:100. They modeled the clot as a fractal mesh, in agreement with recent results using alternative measurement techniques (11).

Sizes of fibers

The average diameter of fibrin fibers has been estimated under varying conditions by means of turbidimetry (16), electron microscopy (21–24), and light-scattering techniques (17–19,25). Results show that the fiber width varies widely with polymerization conditions, such as ionic strength, amount of calcium, type of activating enzyme, and fibrinogen and enzyme concentrations. Diameter measurements estimated by means of turbidity or light-scattering data are at least three times larger than the diameters seen in electron microscope (EM) micrographs. Because electron beams are

Submitted February 5, 2010, and accepted for publication April 26, 2010.

*Correspondence: catonf@ujf-grenoble.fr

Editor: Roberto Dominguez.

0006-3495/10/10/2018/10 $2.00

doi: 10.1016/j.bpj.2010.04.059

strongly absorbed by water, near-vacuum conditions are required for EM. Therefore, the EM measurements are made on clots that have a large portion of their solvent removed. Because the solvent content of fibrin fibers is normally at least 70%, EM measurements are probably more closely related to the actual amount of protein in the fibers rather than to the fibers' actual size.

Density of fibers

Turbidimetry (11,14–16,26,27), light-scattering techniques (25,28), and refractive index matching (29) have been used to evaluate the protein concentration of the fibers in fibrin clots. Results suggest that proteins make up, at most, 30% of the volume of a fiber. Light-scattering experiments (25,28) and experiments based on refractive index matching (29) suggested that the protein concentration is strongly dependent on the ionic strength, in contrast with results reported from turbidity measurements (16). Until now, it has been difficult to extract clear trends from data available in the literature.

Nanostructure: Internal lateral structure

Few studies have attempted to study the internal structure of fibers, especially from the experimental point of view. Some of the most important results regarding this internal structure come from theoretical studies by Hermans (30), Weisel (24), and Yang et al. (3). Their three structural models are similar and aim to explain the fact that the solvent content in fibrin fibers is unusually large (80%). The most recent structural model (3) shows a quasicrystalline order with a tetragonal cell of $19 \times 19 \times 45$ nm, where $a = 19$ nm corresponds to twice the distance between protofibrils and $c = 45$ nm corresponds to the length of a monomer. Experimentally, two recent investigations advocate a random lateral structure (4,5), while two small-angle x-ray scattering (SAXS) studies of fibrin films seem to favor lateral crystal structures (2,31). The most recent study (32) performed using small angle neutron scattering on deuterated clots did not provide a clear description of the internal structure of the fibers. Specifically, although the study has a clear fundamental interest, the clots used in the experiments were made using conditions that were far outside the physiological regime. Very high ionic strengths (>1000 mOsm), very high fibrinogen concentrations ($\leq$70 mg/mL), and very low thrombin concentrations (0.16 IU) were used. Consequently, results based on fibers made under these conditions are difficult to compare to those of studies concerned with quasiphysiological conditions. For example, the radii of the fibers were found to be independent of the concentration of fibrinogen. This is in plain contradiction with Ferri et al. (1).

Objectives

As can be seen from this brief review, experimental data concerning the internal nanostructure of fibrin fibers is scarce. However, it is clear that if accurate and physiologically relevant measurements of both the radius of the fibers and their density were available, conclusions that are more reliable could be reached. The first goal of this article is to demonstrate how to extract this information reliably from properly analyzed light spectroscopy data. The second goal is to reach a realistic picture of a fiber's structure in conditions that are relevant from both biological and chemical points of view.

After describing the sample preparation, we will show how to link light spectra to fiber structure and then validate the structural characterizations using small-angle light-scattering (SALS) and dynamic light-scattering (DLS) data. We will then explore the dependence of the internal structure of the fibers upon the external reaction conditions.

MATERIALS AND METHODS

Sample preparation

Human thrombin was purchased from Cryopep (Montpellier, France) as a solution of 12 μL containing 366.4 IU. The material was diluted in nanopure water to a concentration of 0.4 IU/μL, then divided into 25-μL aliquots and finally frozen at -80°C. Human fibrinogen was a generous gift from the Laboratoire Francais du Fractionnement et des Biotechnologies (Les Ulis, France). The lyophilized powder was dissolved in 100 mL of nanopure water to a final concentration of 14.8 mg/mL, then divided into 1-mL aliquots and finally frozen at -80°C. Before use, thrombin and fibrinogen aliquots were thawed to room temperature (25°C) in a 37°C water bath for 5 min. Then the temperature was equilibrated at 25°C for 15 min. Finally, the aliquots were diluted in the appropriate buffered solution to twice the desired final concentration. Clots were prepared from mixtures that typically contained 0.1–1 mg/mL fibrinogen. Fibrinogen was activated using 0.1–1 IU/mL thrombin. Polymerizations were carried out in HEPES buffer with varying NaCl concentrations. This yielded solutions with ionic strengths ranging from 75 mOsm to 600 mOsm. Fibrin gels were formed directly in 10-mm thick polystyrene cuvettes by mixing 1 mL of the fibrinogen solution and 1 mL of the thrombin solution.

Spectrophotometer

After 90 min, optical density measurements were made at 25°C with a UV mC^2 single-beam scanning spectrophotometer (SAFAS, Monaco). The wavelength ranged from 500 nm to 800 nm with a bandwidth of 10 nm and an acquisition time of 0.1 s. Ten cuvettes were measured simultaneously.

The reference optical density was taken from a buffer measurement.

Data analysis

Data reduction

Each data point in all the graphs represents numerous replicated clotting experiments (at least 13 experiments, but typically 20 experiments). Each data point and its standard deviation were calculated from these replicates. The average mass/length ratio, μ, and the average radius, a, of the fibrin fibers were determined from the theoretical considerations of the next section, using the following method. Plotting $\tau\lambda^5$ as a function of λ^2 gives a straight line whose slope yields the mass/length ratio (μ). The ordinate at the origin gives the square of the average radius. For most polymerization

conditions, plots of $\tau\lambda^5$ versus λ^2 could be fit with straight lines. This is in agreement with our model. However, for ionic strengths >300 mOsm, the spectra often showed peaks. All results shown below are calculated only from data with a straight line trend.

Nanostructure parameters

A quantity often used to describe the fibrin fibers is the average number of protofibrils per cross section. This is determined from μ only by

$$Np = \frac{\mu}{\mu_0},$$

where $\mu_0 = 144.10^{11}$ Da/cm is the mass/length ratio of a single protofibril (16,25). This quantity does not provide information regarding the inside packing of the fibers because it depends not only on the number of protofibrils but also on the size of the fiber. Several other quantities can be used to describe this packing.

A particularly relevant quantity is the average distance between the protofibrils. This can be determined from the spectra measurements in the following way. Fibers of radius a and protein mass concentration δ are made by n protofibrils packed at an average distance z from each other. Each protofibril is thus at the center of a virtual cylinder of radius $z/2$, the virtual cylinders being at best on a hexagonal lattice with a density of $\phi_{hex} = 0.9$. The definition of packing is

$$\phi_{hex} = \frac{\pi z^2}{4} n_d,$$

with n_d as the number density of the cylinders. The quantity z is then expressed as

$$z = \sqrt{\frac{\mu_0}{\delta}}.$$

Assuming a random packing fraction changes the result only by a few percent, the average protein mass concentration in the fibers (δ) is simply determined from the mass/length ratio and the radius of the fibers as

$$\delta = \frac{\mu}{\pi a^2}.$$

Small-angle x-ray scattering

Experimental details

Because we aimed to determine the nanostructure of the fibrin fibers, we performed several small-angle x-ray scattering (SAXS) experiments at the ID02 line at the European Synchrotron Radiation Facility in Grenoble, France. Two clots were formed at 1 mg/mL fibrinogen and 1 UI/mL thrombin in the same buffer as above at an ionic strength of 300 mOsm. After quickly mixing equal quantities of fibrinogen and thrombin solutions, this reaction solution was injected into 1.5-mm diameter polycarbonate capillaries using a sterile syringe. The clots were allowed to form for 90 min before SAXS measurement. The sample/detector distance was set at 2 m for one sample and at 10 m for the other. The acquisition time was set to 0.1 s so that no radiation damage occurred. Ten points were scanned along the length of the tube.

Data reduction

The acquired images were axisymmetric, indicating no preferential alignment direction of the fibers. The images were angularly averaged. The background noise was measured from the same tubes filled only with buffer and was then subtracted from the averaged image. Finally, because no significant variation was observed along the length of the tube, the 10 images were also averaged.

THEORY: MODELING OF THE OPTICAL DENSITY OF A FIBRIN CLOT

In this section, we first provide the rigorous definition of the turbidity with respect to the optical density of a solution. A quantitative expression for the model of the optical density of a formed fibrin clot is then provided.

Optical density and turbidity are generally not proportional

As explained in the Introduction, taking turbidity measurements of clots is a technique almost as old as the study of clotting itself. Indeed, the terms ''turbidity'' and ''optical density'' are often assumed to be different ways to denote the same thing. For example, in their seminal article (181 citations to date), Carr and Hermans (16) wrote: ''The turbidity is, of course, equal to the ratio of optical density to sample thickness multiplied by Ln (10).'' As we will now show, this is true only for very large dilutions and is not true for most experiments on clot formation. The optical density of a solution, D, is the intensity decrease of the transmitted light in decimal logarithm units,

$$\frac{I_t}{I_0} = 10^{-D.A} \ or, \ D.A = -\log\left(\frac{I_t}{I_0}\right), \tag{1}$$

where I_0 is the incident light intensity and I_t is the transmitted (measured) light intensity. The quantity A is the sample thickness in centimeters, so D is in units of cm^{-1}.

As long as the solid angle of the detector is small (which is usually the case), the measured intensity is simply the incident intensity minus the total absorbed and scattered light. Supposing for simplicity that absorption is negligible,

$$I_t = I_0 - 2\pi \int_0^{\pi} I_\theta . sin\theta \, d\theta = I_0(1-\tau). \tag{2}$$

The right-hand side of Eq. 2 defines the turbidity as

$$\tau = 2\pi \int_0^{\pi} \frac{I_\theta}{I_0} sin\theta \, d\theta.$$

Using Eqs. 1 and 2, for a standard thickness of one centimeter, we get

$$\tau = 1 - \exp(-D.\ln(10)). \tag{3}$$

Performing a Taylor expansion of ~1 in –D. ln(10) of Eq. 3, one obtains

$$\tau = D.\ln(10). \tag{4}$$

This relation is the mathematical embodiment of the above quote from Carr and Hermans, which is thus valid only when $\tau << 1$. In other words, the relation $\tau = D.$ ln(10) is an approximation that can be applied only in the limit of vanishing optical densities or turbidities. However, this

approximation has been used far outside its validity domain (e.g., Carr and Hermans (16) and subsequent work), where optical densities are commonly ~1. Equation 3 shows a straightforward way of avoiding the use of the above Taylor expansion because this equation allows calculation without any approximation of the turbidity from the optical density.

Turbidity of a solution of randomly oriented fibers

For a solution of randomly oriented fibers of long and thin rods, the turbidity is (e.g., Carr and Hermans (16))

$$\tau\lambda^5 = 2\pi^3 C n_s \mu \left(\frac{dn}{dc}\right)^2 \frac{44}{15}\left(\lambda^2 - \frac{184}{154}\pi^2 a^2 n_s^2\right), \quad (5)$$

where N is Avogadro's number, λ is the incident wavelength [cm], $\mu = m_f/L$ with m_f the protein mass in a fiber [Da] of length L [cm] and radius a [cm], C the initial fibrinogen mass concentration [g.mL^{-1}], and $n_s = 1.33$, $dn/dc = 0.17594$ cm^3 g^{-1} (33). As discussed in the Appendix, this expression is valid for our experimental conditions whereas the expression used by Carr and Hermans (16) is not.

VALIDATION: COMPARISON OF DIFFERENT SCATTERING MEASUREMENTS

Average radius

To check the method proposed in this article, we reproduced experiments where the average radius of the fibers from formed clots was measured using a specially developed SALS setup (19). The results from our experiments together with those of Ferri et al. (19) are presented in Fig. 1. There is perfect agreement between the SALS measurements and the light spectroscopy measurements. This agreement is even more convincing when it is considered that each of our data points represents an average of at least 15 clots while the SALS data represent a single clot. In contrast, if we apply the formula of Carr and Hermans (16) to our raw data (*shaded squares* in Fig. 1), the agreement is considerably poorer. Even the trend is incorrect, as the radius seems to decrease with the fibrinogen concentration.

Number of protofibrils

Although there have been several measurements of the number of protofibrils (or the mass/length ratio) in the fibers (e.g., (11,12,15,16,26,27,34), most of them are based on the work of Carr and Hermans (16) and thus cannot be used to further validate our modified procedures. An alternative measurement of the number of protofibrils was made by Papi et al. (28) using DLS, a technically different method. Our measurements are similar to those in the study by Papi et al. (28) although the fibrinogen concentration is not precisely known in that study. The comparison shown in Fig. 2 shows excellent agreement between the two methods. We also compared our complete calculation and the approximate calculation from Carr and Hermans (16). Below 300 mOsm, the difference is quite significant, amounting to approximately a factor of two, while at higher ionic strength the Carr calculation also yields the correct trend and correct values. Finally, we calculated the number of protofibrils using the three formulae for the same data used to generate Fig. 1. In Fig. 3, we see that while the estimate from Carr's original article fits well (this formula was only used by Wolberg et al. (27)), the estimates using the simplified version (12) are too low by a factor of two.

In conclusion, the corrections to previous calculations of fiber nanostructure provided in this article yield reliable and robust results that agree quantitatively with both SALS and DLS data. Furthermore, we show that the light spectroscopy method is able to provide, simultaneously, the average radius of fibers and the average number of protofibrils inside those fibers. We will now use this method and SAXS

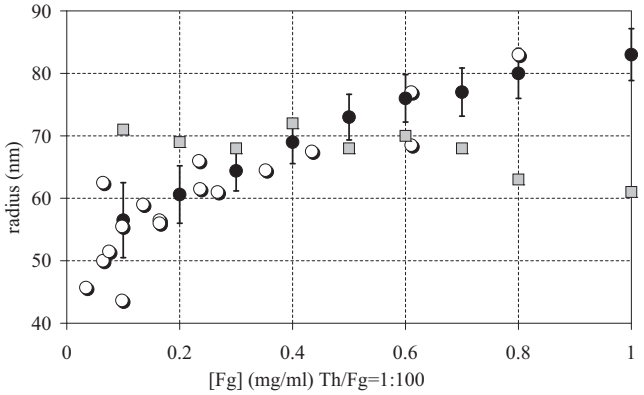

FIGURE 1 Average fiber radius versus [Fg], IIa/[Fg] = 10^{-2}, 300 mOsm. (*Solid circles*) This article. (*Open circles*) Data from Ferri et al. (19). (*Shaded squares*) Our data analyzed with the formula from Carr and Hermans (16).

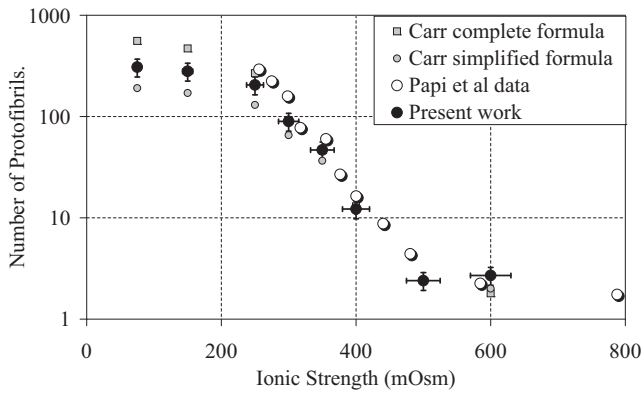

FIGURE 2 Average number of protofibrils in the fibers versus the ionic strength ([Fg] = 1 mg/mL, IIa 1 UI/mL). (*Solid circles*) This article. (*Shaded squares*) Carr complete formula. (*Open circles*) Papi et al. (28). (*Shaded circles*) Carr approximate formula.

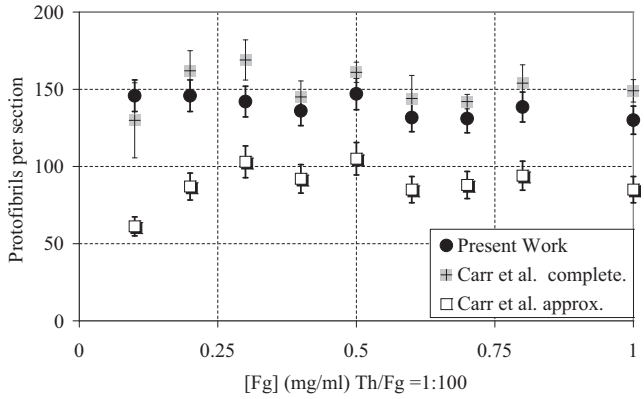

FIGURE 3 Plot of the average number of protofibrils in the fibers versus [Fg], IIa/[Fg] = 10^{-2}, 300 mOsm. (*Solid circles*) This article. (*Shaded squares*) Carr complete formula. (*Open squares*) Carr's simplified formula at 350 nm.

measurements to explore the nanostructure of fibrin clots under varying conditions.

NANOSTRUCTURE OF FIBRIN CLOTS

The structure of formed fibrin clots is known to depend on many factors including thrombin and fibrinogen concentrations, ionic strength and content, etc. To better understand and ultimately model the interplay between these factors and fibrin polymerization, we choose to simplify the factors as much as possible. In particular, the first (enzymatic) step is well understood and has better models associated with it compared to the subsequent aggregation.

The catalytic range

This first step is a double enzymatic reaction where the fibrinopeptides A and B are cleaved at different rates (35,36). Neglecting the influence of fibrinopeptide B, the generation of a fibrine monomer can be described formally by the Briggs-Haldane equation,

$$\frac{d\overline{S}}{dt} = \frac{k_2 E_T}{1 + \frac{E_T}{\overline{S}} + \frac{K_m}{\overline{S}}}, \tag{6}$$

where $\overline{S} = S + C$ is the total quantity of unreacted fibrinogen (37), and k_2 and K_m are the reaction constants. Because this equation can demonstrate complex behaviors, we choose to stay in the regime where $E_T/\overline{S} \ll 1$ and $K_m/\overline{S} \gg 1$, a regime that simplifies the above equation into the usual form:

$$\frac{d\overline{S}}{dt} = \frac{k_2}{K_m} E_T \overline{S}. \tag{7}$$

As the above conditions concern only the total remaining substrate, it is sufficient that we satisfy the conditions only at the start of the experiments. We thus fix $S/E = 100$.

In the next section, we first discuss the results from two SAXS measurements taken under a single condition within this catalytic regime. This will give us a framework to discuss subsequent results.

Nanostructure from SAXS spectra

The two spectra obtained for the same clotting conditions (IIa: 1 UI and [Fg] = 1 mg/mL) at two distances (2 m and 10 m) are merged and shown as a single curve in Fig. 4. The good superposition in the overlapping domain in Fig. 4 indicates that there is high experimental reproducibility (no shift was applied to the *curves*).

The shape of this spectrum (Fig. 4) is similar to the shapes of spectra obtained by Missori et al. (31) and Weigandt et al. (32). The data span 2.5 decades of q, from 0.02 nm^{-1} to 3 nm^{-1}, corresponding to a scale that ranges from 300 nm to 2 nm. This spectrum thus complements the SALS spectrum of Ferri et al. (18). At a scale of 80 nm, we observe a curvature change. This is likely indicative of a transition to the larger scale fractal structure as found by Ferri et al. (18) and Weigandt et al. (32). The change should occur at a wavelength that is close to the average radius of the fibers. Indeed, 80 nm is close to our spectroscopically determined radius of 75 nm. At smaller q, the curve is similar to the solvent-fiber Porod regime found by Weigandt et al. (32).

Concerning the nanostructure of the fibers, three sharp peaks and two broad peaks are found in Fig. 4. Because the half-width of the sharp peaks yields a coherence length of 300 nm, these peaks are related to the fibers' longitudinal structures.

Longitudinal structure

The first sharp peak in Fig. 4 lies at $q = 0.282$ nm^{-1}, which translates to the usual longitudinal periodicity of 22.25 nm. The second peak lies at $q = 0.849 = 3 * 0.282$ nm^{-1}, which is exactly three times the wavenumber of the main periodicity. The last peak is located at $q = 1.127$ nm^{-1}. This

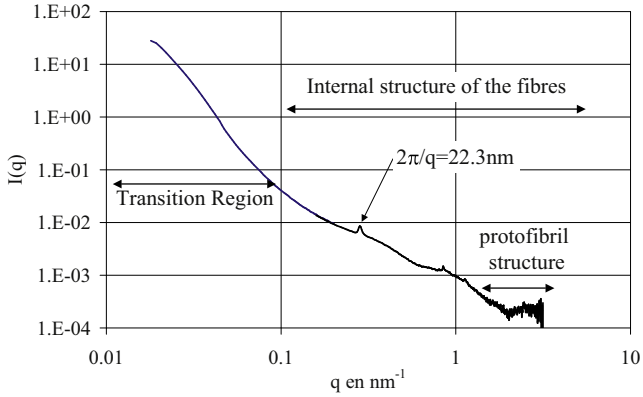

FIGURE 4 SAXS spectrum of two clots in the same reaction conditions in logarithm scale (IIa: 1 UI/mL, [F]: 1 mg/mL [F], 300 mOsm). (*Arrows*) Main features of the internal structure of the fiber.

peak may be the fourth harmonic $q = 4 * 0.282 = 1.13$ of the 22.25-nm fundamental. It may also correspond to the second periodicity found in the micrographs from transmission electron micrography (e.g., Weisel (24)). The presence of these three well-defined, sharp peaks with large coherence lengths (300 nm) indicates that the 22.25-nm periodicity is a very strong geometrical feature of the fibers.

Lateral structure

Because SAXS is mainly sensitive to the mass distribution, if the fibers' lateral structure is crystalline with a basic cell, Bragg peaks at q vectors corresponding to those distances would be present. Further, the half-width of these Bragg peaks would correspond to the diameter of the fibers (38,39). In contrast, the additional peak observed between 12 nm and 6 nm in Fig. 4 is quite broad with a small coherence length (between 10 and 30 nm). This peak is much smaller than the average radius of the fibers (75 nm in this case). A second, smaller broad peak is observed. This peak extends from 22.25 nm to 15 nm. Its position corresponds roughly to the sharp peak observed by Torbet et al. (39) on oriented fibrin fibers and to the broad peak noted in the unoriented clots observed by Missori et al. (31). This broad peak cannot be the fundamental of the first broad peak, as the 12–6-nm broad peak has a greater intensity and the range of q extends below the third harmonic of 22.25 nm. Both of these broad peaks likely correspond to a partial ordering of protofibrils inside fibers. If this is the case, then these protofibrils would be separated by distances of ~8–10 nm and 15–22.5 nm. This is in agreement with the average protofibril-to-protofibril distance (8 nm) and cell periodicity (19 nm) taken from the structural models of Yang et al. (3) and Weisel (24).

A complementary interpretation of this structure arises if the possibility is considered that the baseline drawn in Fig. 4 between $q = 0.14$ nm^{-1} and $q = 2$ nm^{-1} represents the underlying lateral structure. In this case, the lateral structure would be fractal with a dimension of 5/3. This interpretation is in agreement with the work of Guthold et al. (4), who used very different methods to deduce the existence of an internal fractal structure.

In conclusion, our tentative interpretation of the above SAXS spectra demonstrates a longitudinal periodicity corresponding to the well-known, half-staggered periodicity of 22.25 nm. On the other hand, the broad peaks observed for sizes between 6 nm and 19 nm appear to be related to the lateral nanostructure of the fibers. Under these conditions ([IIa] = 1 UI; [Fg] = 1 mg/mL), the protofibril arrangement may be interpreted as a crystal with many holes or as a fractal structure. These are two different views of the same structure.

Nanostructure from light spectroscopy: internal lateral structure

The SAXS results were obtained under a single condition. The analysis yielded strong indications that there is a disjointed inner structure of fibers. Although these results are promising, they must be confirmed and expanded upon using a different method. We will now explore the influence of the reaction environment (fibrinogen concentration and ionic strength) on the nanostructure of clots using the light-spectroscopy method.

Fibrinogen concentration at [Th]/[Fg] = 1/100

The average fiber radii measured at different fibrinogen concentrations and for two different ionic strengths are shown in Fig. 5.

At both 300 mOsm and 75 mOsm, the average radius is an increasing, almost linear, function of the fibrinogen concentration. This is in perfect agreement with the results of Ferri et al. (18). There is little variation in the number of protofibrils per cross section for fibers made with different concentrations of fibrinogen (*inset graph* in Fig. 5). The number of protofibrils appears to be mainly controlled by the ionic strength. There are more than twice as many protofibrils at 75 mOsm than there are at 300 mOsm (also see the next section). To better understand this result, the average distance between the protofibrils is plotted in Fig. 6. This figure indicates that the average distance increases proportionally with the fibrinogen concentration. The distance is larger for higher ionic strengths. This result is incompatible with a pure quasicrystalline structure in which the average distance between protofibrils would remain constant. If the fibers were crystalline, the number of protofibrils would simply be the number of protofibrils per unit cell multiplied by the number of unit cells in the fiber:

$$Np = \pi r^2 / Surface_{cell}.Np_{cell}.$$

This number would thus increase as the square of the radius of the fibers. For instance, using the model of Yang et al. (3), a crystalline fiber of 83 nm radius formed at Fg = 1 mg/mL and 300 mOsm would have 240 protofibrils packed inside of

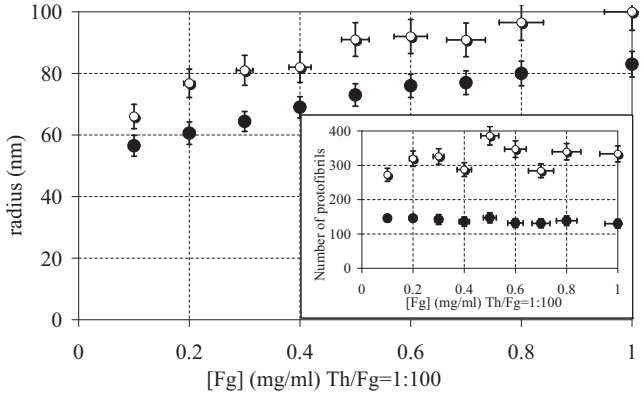

FIGURE 5 Average fiber radius in the catalytic regime versus [Fg] under ionic strength of 300 mOsm (*solid circles*) and 75 mOsm (*open circles*). (*Inset*, *graph*) Average number of protofibrils per cross section under the same conditions.

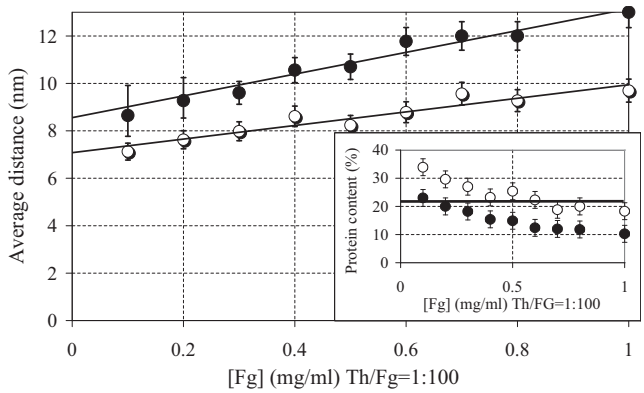

FIGURE 6 Average interprotofibril distance versus [Fg] in the catalytic regime under ionic strength of 300 mOsm (*solid circles*) and 75 mOsm (*open circles*). (*Inset*) Protein content versus [Fg]. The bold line corresponds to the density predicted by the model of Yang et al. (3).

it, whereas only 130 are found. This is nearly a 50% difference. The protein content inside the fibers is plotted in the inset of Fig. 6. We find that at physiologically relevant ionic strength, the highest fiber densities are approximately 20% (80% solvent content). This agrees with Carr and Hermans (16) as well as with the different structural models (3,24,30).

To rationalize this result, we propose the following modification of the model of Yang et al. (3). First, in Fig. 7 *a*, we show a schematic representation of the nanostructure of a hypothetical fiber of radius 40 nm, following the model proposed by Yang et al. (3). The dark objects are in the plane of observation, whereas the light ones are 22.5 nm below it. According to the model of Yang et al. (3), such a fiber of 40-nm radius contains ~60 protofibrils. The density of this fiber corresponds to that formed at [Fg] = 0.2 mg/mL, 300 mOsm.

In Fig. 7 *b*, 25% of the protofibrils have been removed. This corresponds to the density fibers formed under conditions of [Fg] = 0.5 mg/mL and 300 mOsm. Already, a disjointed picture of fibril nanostructure is appearing. If 50% of the protofibrils are removed, a structure is obtained that resembles the one drawn in Fig. 7 *c*). This corresponds to the density of fibers observed under conditions of 1 [Fg] and 300 mOsm. In this figure, a fairly clear fractal mesh is observed. As a final indicator, the average protofibril-protofibril distance at very low concentrations seems to converge to a value of 8.5 nm (see Fig. 6), a value that is close to the distances calculated in the model of Yang et al. (3). These findings can be interpreted if we use a framework in which the lateral structure of fibers is locally crystalline, but contains a large number of holes that increase with the fibrinogen concentration. Visually, this structure looks very much like that of a fractal network.

Finally, the reader may have observed that the density of the fibers at 75 mOsm is twice as large as the density at 300 mOsm (*inset* of Fig. 6) and that the average distance at very low concentrations converges to a lower value of 7.5 nm. It appears that the ionic strength of the environment strongly influences the nanostructure of the fibers. We will now investigate this more closely.

Ionic strength, [Fg] = 1 mg/mL and [IIa] = 1 UI/mL

To further examine the influence of the reaction environment on the fibers nanostructure, experiments were performed at several ionic strengths with constant [Fg] = 1 mg/mL and [IIa] = 1 UI/mL. These values are in the catalytic range.

We first plot the evolution of the radius and the number of protofibrils per fiber cross section. The data for the protofibril numbers are the same data that were successfully compared to the results of Papi et al. (28) (see Number of Protofibrils).

We first observe in Fig. 8 that the number of protofibrils decreases as a function of the ionic strength. Above 400 mOsm, only a very small number of protofibrils are found in the fibers, which is in agreement with the works of Hantgan and Hermans (21) and Papi et al. (28). By plotting the evolution of the radius and the interprotofibril distance of these fibers as functions of the ionic strength (Fig. 9), a clear picture of the internal structure of the fibers can be drawn. Indeed, at high ionic strength (400 mOsm), the fibers are composed of only one or two protofibrils but their radius remains above 50 nm and the interprotofibrils distance is even larger (55 nm). This suggests that a dramatic structural transition occurs at an ionic strength close to 400 mOsm. Because the fibers are composed of only one or two protofibrils when the ionic strength is so high, they likely form a twisted, ladderlike shape. Conversely, at low ionic strengths, more protofibrils are present inside the fibers. Similarly, for decreasing ionic strength, the radius increases from 62 nm to 100 nm while the interprotofibril distance regularly decreases from 22.5 nm to 10 nm. In other words,

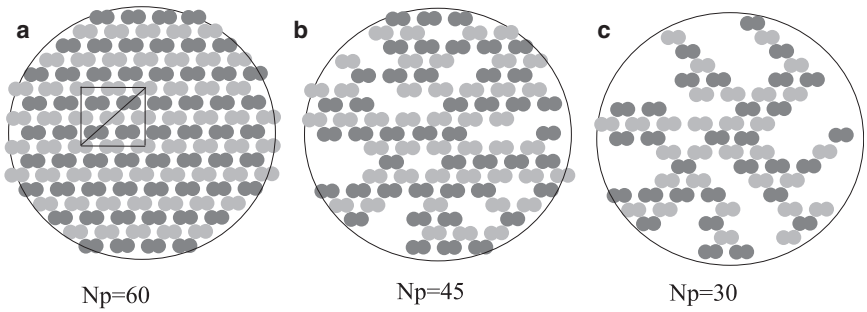

FIGURE 7 Schematic of the internal structure of a fibrin fiber of diameter 75 nm using the model of Yang et al. (3). (*a*) Crystalline structure with a number of protofibrils of 60 (maximum possible density). (*b*) Structure with 25% of protofibrils removed with respect to panel *a*. (*c*) Structure with 50% of protofibrils removed with respect to panel *a*. This corresponds to the highest density measured with light spectroscopy.

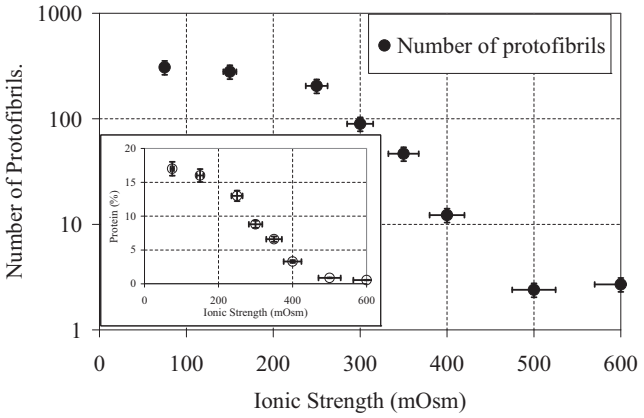

FIGURE 8 Average number of protofibrils and protein mass concentration versus the ionic strength. [Fg] = 1 mg/mL and [IIa] = 1UI/mL. (*Inset*) Evolution of the protein concentration.

as the fibers become larger because of decreased ionic strength, they also become increasingly dense. Incidentally, because the total initial number of monomers is constant in each trial, the total length of fibers must decrease. One way this can occur is if the fractal dimension of the network formed by the fibers decreases. This hypothesis is supported by qualitative observations of Papi et al. (28).

CONCLUSION

We have shown that the correct analysis of spectrometric data obtained from formed clots allows the simultaneous determination of the average radius and density of the fibrin fibers present in the clot, in excellent agreement with SALS and DLS results. This spectrometry complements existing data and allows us to draw a clearer picture of the fibrin fibers' structure. Using this corrected method, we show the major role played by the ionic strength of the solution in forming the nanostructure of the fibers.

Using this technique, we find that at ionic strengths <400 mOsm, fibers have a disjointed structure with a local crystalline arrangement. This picture is supported by SAXS spectra suggesting that this lateral internal structure may even be a two-dimensional fractal. A dramatic structural change is observed for ionic strengths >400 mOsm, above which the fibers seem to be composed of only one ladderlike, twisted structure.

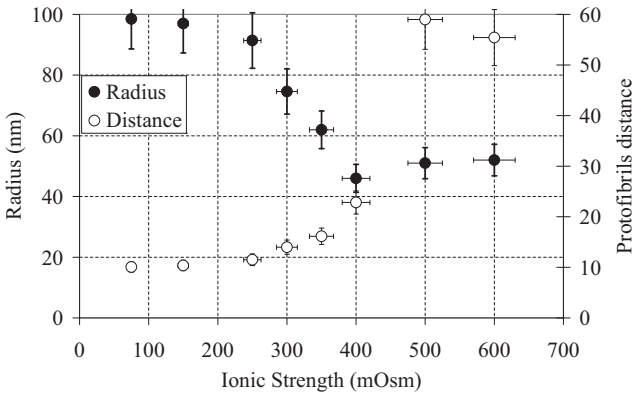

FIGURE 9 Average radius and interprotofibril distance versus the ionic strengths. [Fg] = 1 mg/mL and [IIa] = 1 UI/mL.

Finally, it is worth noting that the clot characterizations proposed in this study are not proposed in qualitative terms (e.g., thin or coarse), but in quantitative terms using easily understandable quantities such as the fibers' average radius and density. As such, the approach proposed here may be an excellent medical tool.

APPENDIX: VALIDITY OF APPROXIMATIONS

Several approximations were used to obtain Eq. 5. First, the optical index ratio between the particles and their suspending medium must be sufficiently small (the Rayleigh-Gans-Debye approximation). Further, the fiber radius must be sufficiently small with respect to the wavelength and the length must be sufficiently large with respect to the wavelength. Finally, the concentration must be sufficiently small that the structure factor can be neglected. To check that the calculations are consistent and can be applied to formed clots, we review here the validity of these approximations in detail.

Rayleigh-Gans-Debye approximation

By comparing the Rayleigh-Gans-Debye approximation with that of Shifrin (from Bishop (40)), we determined that if

$$m_a = \frac{m_p}{m_s},$$

the ratio of the index of refraction of the particle m_p to the index of refraction of the surrounding medium is close to 1, i.e., the Rayleigh-Gans-Debye approximation is valid. Because fibrinogen is a protein, according to Ferri et al. (1), $m_a \simeq 1.05$ (mean $\pm$ SE ~1%).

Asymptotic expansions: long and thin rods with respect to the wavelength

For several values of λ, a, and L, the approximated integrals were calculated numerically. If higher-order terms are neglected, Eq. 5 will yield <10% error. This is valid as long as the average fiber length is >800 nm and the average radius of the fibers is <100 nm. Experimentally, the average length of the fibers cannot be determined using this method. However, it is well known that the fiber lengths are usually ~10 μm, i.e., much larger than the minimum length required for the model to be applicable.

Structure factor

In our calculations, the structure factor, $S(\theta)$, was neglected. To evaluate this approximation, we used the complete

multiscale fractal model of the fibrin clot build and applied it to the light-scattering data of Ferri et al. (18). In this model, the structure factor is given by

$$S(\theta) = 1 - e^{-(0.28Lq)^2} \text{ with } L = \textit{fiberlenth } [cm] \text{ and } q = \textit{wave vector } \left[cm^{-1}\right].$$

In our setup, the equivalent wave-vector range varies from

$$q_{min} = \frac{2\pi}{\lambda_{max}} = 7.9\cdot 10^4 \mathrm{cm}^{-1} \text{ to } q_{max} = \frac{2\pi}{\lambda_{\min}} = 1.3\cdot 10^5 \mathrm{cm}^{-1}.$$

As a consequence, $S(\theta) = 1$. In other words, because of the accessible range of wave vectors, the large-scale structure does not influence the measurements. Thus, the structure factor is indeed negligible.

Inappropriate approximation in Carr and Hermans' work

To obtain an expression that is suitable for determination of the radius and the mass/length ratio, Carr and Hermans (16) use the following series expansion (Eq. 6):

$$\left(1 - \frac{184}{154}\pi^2 n^2 \frac{a^2}{\lambda^2}\right)^{-1} = \left(1 + \frac{184}{154}\pi^2 n^2 \frac{a^2}{\lambda^2}\right).$$

Because clots were scanned from 400 nm to 800 nm and the fiber radius is $\simeq$70 nm, this Taylor expansion is not valid. However, when this expansion is added to the previous approximation, it produces plots of $1/\tau\lambda^3$ as a function of $1/\lambda^2$ that are straight lines. It also produces a very small intercept at the origin—which suggested that the influence of the radius on the curves is small and can be neglected. As we see in the Conclusion, the correct calculation shows that this is not true.

Polydispersity

In all calculations, the form factor is first averaged over all directions. Then it is averaged over the whole measurement volume. This yields the mass concentration dependence. Thus, the size and density parameters are volume-averaged parameters.

We thank J. Oberdisse, E. DiCola, and Y. Rharbi for their kind help in interpreting the SAXS spectra.

REFERENCES

1. Ferri, F., M. Greco, and M. Rocco. 2001. On the determination of the average molecular weight, radius of gyration, and mass/length ratio of polydisperse solutions of polymerizing rod-like macromolecular monomers by multi-angle static light scattering. *Macromol. Symp.* 162:23–44.
2. Caracciolo, G., M. D. Spirito, …, R. Arcovito. 2003. Protofibrils within fibrin fibers are packed together in a regular array. *Thromb. Haemost.* 89:632–636.
3. Yang, Z., I. Mochalkin, and R. F. Doolittle. 2000. A model of fibrin formation based on crystal structures of fibrinogen and fibrin fragments complexed with synthetic peptides. *Proc. Natl. Acad. Sci. USA.* 97:14156–14161.
4. Guthold, M., W. Liu, …, R. Superfine. 2004. Visualization and mechanical manipulations of individual fibrin fibers suggest that fiber cross section has fractal dimension 1.3. *Biophys. J.* 87:4226–4236.
5. Hunziker, E. B., P. W. Straub, and A. Haeberlis. 1990. A new concept of fibrin formation based upon the linear growth of interlacing and branching polymers and molecular alignment into interlocked single-stranded segments. *J. Biol. Chem.* 265:7455–7463.
6. Klinke, K. 1931. Coagulation studies. III. Communication. Methodology for the tyndallometry of light-absorbing liquids. *Res. Exp. Med. (Berl.).* 77:718–725.
7. Klinke, K. 1931. New investigations into the second phase of blood coagulation. *Klin. Wochenschr.* 10:869–871.
8. Klinke, K., and G. Elias. 1931. Coagulation studies. IV. Communication. Kinetic investigations into fibrinogen clotting. *Res. Exp. Med. (Berl.).* 77:706–716.
9. Ferry, J. D. 1952. The mechanism of polymerization of fibrin. *Proc. Natl. Acad. Sci. USA.* 38:566–569.
10. Ferry, J. D., and P. R. Morrison. 1947. Preparation and properties of serum and plasma proteins. VIII. The conversion of human fibrinogen to fibrin under various conditions. *J. Am. Chem. Soc.* 1947:388–400.
11. Chernysh, I. N., and J. W. Weisel. 2008. Dynamic imaging of fibrin network formation correlated with other measures of polymerization. *Blood.* 111:4854–4861.
12. Weisel, J. W., and C. Nagaswami. 1992. Computer modeling of fibrin polymerization kinetics correlated with electron microscope and turbidity observations: clot structure and assembly are kinetically controlled. *Biophys. J.* 63:111–128.
13. Casassa, E. F. 1955. Light scattering from very long rod-like particles and an application to polymerized fibrinogen. *J. Chem. Phys.* 23: 596–597.
14. Carr, M. 1992. Method for determining fibrin fiber size from a single gel optical density measurement. United States Patent No. 5106186.
15. Carr, M. E., and D. A. Gabriel. 1980. Dextran-induced changes in fibrin fiber size and density based on wavelength dependence of gel turbidity. *Macromolecules.* 1980:1473–1477.
16. Carr, M. E., and J. Hermans. 1978. Size and density of fibrin fibers from turbidity. *Macromolecules.* 11:46–50.
17. Bernocco, S., F. Ferri, …, M. Rocco. 2000. Polymerization of rod-like macromolecular monomers studied by stopped-flow, multiangle light scattering: set-up, data processing, and application to fibrin formation. *Biophys. J.* 79:561–583.
18. Ferri, F., M. Greco, …, M. D. Spirito. 2001. Growth kinetics and structure of fibrin gels. *Phys.Rev. E.* 63:1–3.
19. Ferri, F., M. Greco, …, M. Rocco. 2002. Structure of fibrin gels studied by elastic light scattering techniques: dependence of fractal dimension, gel crossover length, fiber diameter, and fiber density on monomer concentration. *Phys. Rev. E Stat. Nonlin. Soft Matter Phys.* 66, 011913.
20. Rocco, M., S. Bernocco, …, F. Ferri. 2006. Early events in the polymerization of fibrin. *Ann. N. Y. Acad. Sci.* 936:167–184.
21. Hantgan, R. R., and J. Hermans. 1979. Assembly of fibrin: a light scattering study. *J. Biol. Chem.* 254:11272–11281.
22. Ryan, E. A., L. F. Mockros, …, L. Lorand. 1999. Structural origins of fibrin clot rheology. *Biophys. J.* 77:2813–2826.
23. Stasio, E. D., C. Nagaswami, …, E. D. Cera. 1998. Cl regulates the structure of the fibrin clot. *Biophys. J.* 75:1973–1979.
24. Weisel, J. W. 1986. Fibrin assembly. Lateral aggregation and the role of the two pairs of fibrinopeptides. *Biophys. J.* 50:1079–1093.
25. DeSpirito, M., G. Arcovito, …, F. Ferris. 2003. Small- and wide-angle elastic light scattering study of fibrin structure. *J. Appl. Crystallogr.* 36:636–641.

26. Carr, M. E., D. A. Gabriel, and J. McDonagh. 1986. Influence of Ca^{2+} on the structure of reptilase-derived and thrombin-derived fibrin gels. *Biochem. J.* 239:513–516.

27. Wolberg, A. S., D. A. Gabriel, and M. Hoffman. 2002. Analyzing fibrin clot structure using a microplate reader. *Blood Coagul. Fibrinolysis.* 13:533–539.

28. Papi, M., G. Arcovito, …, G. Boumis. 2005. Simultaneous static and dynamic light scattering approach to the characterization of the different fibrin gel structures occurring by changing chloride concentration. *App. Phys. Lett.* 86, 183901.

29. Voter, W. A., C. L. Veche, and H. P. Erickson. 1986. Concentration of protein in fibrin fibers and fibrinogen polymers determined by refractive index matching. *Biopolymers*. 25:2375–2384.

30. Hermans, J. 1979. Models of fibrin. *Proc. Natl. Acad. Sci. USA.* 76:1189–1193.

31. Missori, M., M. Papi, …, D. Spirito. 2009. Cl^- and F^- anions regulate the architecture of protofibrils in fibrin gel. *Eur. Biophys. J.* 39: 1001–1006.

32. Weigandt, K., D. Pozzo, and L. Porcar. 2009. Structure of high density fibrin networks probed with neutron scattering and rheology. *Soft Matter.* 5:4321–4330.

33. Perlmann, G. E., and L. G. Longsworth. 1948. The specific refractive increment of some purified proteins. *J. Am. Chem. Soc.* 70:2719–2724.

34. Carr, Jr., M. E., R. M. Dent, and S. L. Carr. 1996. Abnormal fibrin structure and inhibition of fibrinolysis in patients with multiple myeloma. *J. Lab. Clin. Med.* 128:83–88.

35. Martinelli, R. A., and H. A. Scheraga. 1980. Steady-state kinetic study of the bovine thrombin-fibrinogen interaction. *Biochemistry.* 1980:2343–2350.

36. Nossel, H. L., A. Hurlet-Jensen, …, R. E. Canfield. 1983. Fibrinopeptide release from fibrinogen. *Ann. NY Acad. Sci.* 408:269–278.

37. Tzafriri, A. R., and E. R. Edelman. 2007. Quasi-steady-state kinetics at enzyme and substrate concentrations in excess of the Michaelis-Menten constant. *J. Theor. Biol.* 245:737–748.

38. Freyssinet, J.-M., J. Torbet, …, G. Maret. 1983. Fibrinogen and fibrin structure and fibrin formation measured by using magnetic orientation. *Proc. Natl. Acad. Sci. USA.* 80:1616–1620.

39. Torbet, J., J. M. Freyssinet, and G. Hudry-Clergeon. 1981. Oriented fibrin gels formed by polymerization in strong magnetic fields. *Nature.* 289:91–93.

40. Bishop, M. F. 1989. Calculations of scattered light from rigid polymers by Shifrin and Rayleigh-Debye approximations. *Biophys. J.* 56: 911–925.